2026 IEEE International Conference on Robotics and Automation (ICRA 2026)
June 1-5, 2026. Vienna, Austria

Feedforward Pressure-Regulated Position Control of Soft Ballooning Actuators Using a Modified Prandtl–Ishlinskii Model

Nashil Sowaruth and Nicolas Herzig*

Abstract— **Thanks to their compliance and adaptability, soft actuators are promising devices for medical applications and the exploration of unstructured environment. However, their nonlinear behaviour, including strong hysteresis effects, presents challenges for accurate position control. This work investigates two data-driven feedforward control strategies for controlling the position of a Hyper-Elastic Ballooning Membrane Actuator (HBMA): a baseline single polynomial fit model and a hysteresis-aware Modified Prandtl-Ishlinskii (MPI) model. Comparative experiments demonstrate that hysteresis-aware control substantially improves accuracy. Specifically, incorporating hysteresis improved overall accuracy by 71% when the HBMA was inflated up to 20.5 mm. During partial inflation-deflation cycles, the MPI controller achieved a mean error of 0.685 mm, corresponding to 9.8% of the 7 mm displacement range. These results highlight the limitations of using feedforward control alone in soft robotic actuation while emphasising the benefits of hysteresis-aware modelling. The findings contribute to the ongoing effort to develop effective control strategies for soft robotic systems.**

I. Introduction

Soft robots, characterised by their compliant and deformable materials, offer significant advantages in safety and adaptability, particularly in the medical field, with applications ranging from haptics and wearables [1] to minimally invasive surgery, implants, and assistive technologies [2], [3]. Their inherent compliance distinguishes them from conventional rigid robots and underpins their growing adoption in scenarios requiring safe human-robot interaction.

Pneumatic actuation is widely used in soft robotics due to its lightweight design, high responsiveness and affordability [4]. Soft pneumatic actuators (SPAs) convert pressurised air into linear or rotational motion and have been applied in wearable exosuits, rehabilitation devices [5], and in delicate medical procedures such as for the augmentation of native blood ejection from the ventricular chambers [6] and colonoscopy [7]. However, SPAs are susceptible to buckling, have non-negligible initial length and low-load bearing capacity. Ballooning membrane actuators [8] offer an alternative design due to their exceptional compliance. These actuators achieve large, reversible deformations, exhibit strong load-bearing capability [9], and reduced buckling instabilities.

From the literature, a handful of ballooning actuators have been proposed, [9] developed a hybrid soft-rigid actuator based on stackable HBMA with a focus to overcome buckling and improving load-bearing. When pressurised, the actuator directs its expansion along a preferred path, enabling measurable displacement. However their modelling approaches remain relatively simple and do not address control challenges arising from nonlinear hysteresis. [10] presented the actuation of a thin flexible end-effector using a pneumatic balloon actuator primarily focus on the material and fabrication. In terms of control and modelling, the authors investigated the mechanical behaviour, but did not develop advanced control strategies for precise position regulation. [11] developed a theoretical exponential growth model for bending-type balloon actuators, relating chamber length, membrane thickness and material properties to bending angle and force generation. While offering useful design insights, the work does not address control implementation. Finally, [8] presented a liquid-driven modelling approach to estimate a ballooning membrane's shape and force output using intrinsic feedback from injected volume and pressure. Their method provides valuable state estimation for contact scenarios but does not explicitly compensate for hysteresis, which they identify as a limitation. Controlled inflation of such actuators has considerable potential for integration into hybrid soft-rigid continuum robots and other soft robotic platforms.

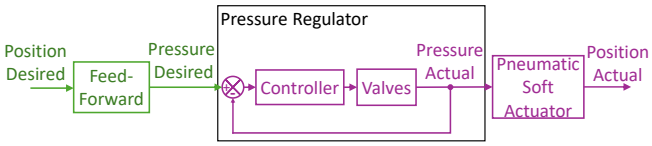

Fig. 1. Control Block Diagram.

Despite significant advancements, precise control of soft actuators remains challenging due to their non-linear mechanics, viscoelasticity, and hysteresis effects. Data-driven approaches offer encouraging outcomes in order to address these non-linearities and enabling a more accurate feedforward control [12]. [13] developed a nonlinear viscoelastic constitutive model for isotropic soft materials, implemented it in finite element analysis, and applied it to study the structural behaviour of pneumatic soft actuators to support design and motion prediction. While to describe hysteresis, several models, including the Preisach model [14], the Prandtl-Ishlinskii (PI) model [15], the Bouc-Wen model [16], and their variations [17] have been employed in soft actuators.

The HBMA exemplifies these challenges. Its high deformability and lack of embedded position sensors render

* This work is supported by the University of Sussex and the Royal Society (RGS/R2/222228)

The authors are with the Department of Engineering and Design, School of Engineering and Informatics, University of Sussex, United Kingdom. n.sowaruth@sussex.ac.uk and n.f.herzig@sussex.ac.uk

direct displacement feedback difficult, making feedforward pressure regulation a compelling control strategy. However, hysteresis in the pressure-position relationship significantly degrades control accuracy, as inflation and deflation follow distinct paths. Simple polynomial fits cannot capture this path-dependent behaviour and therefore struggle to provide accurate predictions across the full actuation range. Furthermore, unlike standard pneumatic artificial muscles, ballooning membrane actuators exhibit snap-through instabilities and extended pressure plateaus. These phenomena create regions of reduced input sensitivity, which further complicates inverse feedforward control.

Recent work by [18] demonstrated that the Modified Prandtl-Ishlinskii (MPI) model can effectively characterise asymmetric hysteresis in Pneumatic Muscle Actuators (PMAs). In their study, the MPI parameters were identified using the Levenberg-Marquardt algorithm and the resulting inverse model was implemented within a cascade control scheme to achieve accurate trajectory tracking despite strong hysteresis. Inspired by this approach, the present study investigates the use of an inverse MPI model for feedforward position control of the HBMA. To the authors' knowledge, this represents the first application of MPI-based hysteresis compensation to ballooning soft pneumatic actuators.

The contributions of this paper are threefold: (1) characterisation of pressure-position behaviour of the soft ballooning membrane actuator, (2) development of two data-driven feedforward position control strategies: a single polynomial fit model and an MPI inverse model, (3) Comparative experimental evaluations of their performance, highlighting the advantages and limitations of each approach. Fig. 1 shows the block diagram of the proposed feedforward control approach.

II. Methods

A. Ballooning Membrane Actuator Fabrication

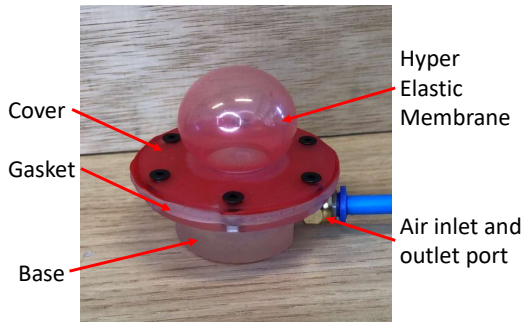

Fig. 2. Soft Actuator Ballooning Membrane

Fig. 2 shows the HBMA, inspired by the design proposed by [9] and [8], that is being investigated in this paper. The base and cover were printed using a resin 3D printer (Formlabs Form 3). Stereolithography printing with Clear resin V4 (Formlabs) was chosen as the material since it offers a printing resolution of 25 microns with a reasonable rigidity and strength suitable to avoid air leakage. A small sheet of commercially available resistance band made of Thermoplastic Elastomer (TPE), with a thickness of 0.50 mm and cut to approximately the same diameter as the cover, was placed between the cover and the base of the HBMA. A 2 mm-thick gasket made of silicone (Ecoflex 00-30) was also placed beneath the TPE membrane, between the cover and the base, to prevent air leakage. The cover, the TPE membrane, and the gasket were all secured to the base with screws. An M5 male-to-6 mm push-in connector was attached to the base to provide a connection port for pneumatic pipes to inject or extract air from the HBMA.

In terms of dimensions, the total height of the assembled cover and base with the ballooning membrane fully deflated is 23.5 mm. Additionally, the outer diameter of the cover and base is 58 mm, while the minor diameter of the orifice, where the soft membrane protrudes, is 20 mm. This diameter was chosen to achieve a noticeable size change in the ballooning membrane when pressurised.

B. Characterisation setup

The characterisation of the HBMA was first carried out to evaluate its inflation behaviour under varying pressure values. From the resulting inflation-deflation loops, two types of data-driven models were derived. First, a single polynomial fit model was obtained by fitting a high-order polynomial to the combined pressure-position data, ignoring hysteresis. Here, position refers to the vertical displacement of the actuator apex (maximum height point) relative to its undeformed baseline, and this definition is used consistently throughout the paper. Second, the loops were used to identify the parameters of a Modified Prandtl-Ishlinskii (MPI) model, which explicitly accounts for hysteresis effects and can be inverted to compute the required pressure for a desired position. Both models were subsequently implemented in feedforward position controllers, where the required pressure is computed as a function of the target position (Figure 1).

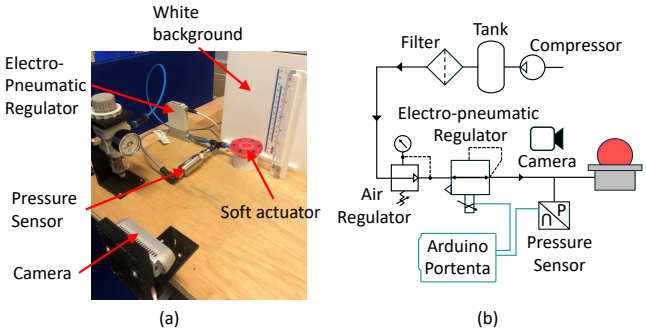

Fig. 3. (a) Real and (b) Schematic Experimental Setup

Fig. 3 depicts the experimental setup for the soft actuator characterisation. The HBMA was connected to an SMC 3.5 L/min electro-pneumatic regulator (SMC ITV0010-3BS), which regulates pressurised air from an air compressor. The electro-pneumatic regulator, with a pressure output range of 0.01 to 1 bar, was controlled via an Arduino Portenta Machine Control, which commanded the pressure regulator

through a series of pressure sweeps while logging pressure sensor data. The internal pressure of the ballooning membrane was measured using a pressure sensor (RS 175-4984), with a range of 0 to 1 bar. The pressure data was recorded by the Arduino with an acquisition rate of approximately 7.5 Hz, which was limited by the serial communication and logging routine of the microcontroller rather than the pressure sensor itself. An RGB-D camera (Intel RealSense D435i) was used to capture the position of the membrane at 30 fps. The actuator position was computed as the vertical displacement of the membrane apex relative to its undeformed baseline, obtained from the RGB image after segmentation of the membrane region of interest. MATLAB (R2023a) was used to collect the camera images, with the position data recorded in a CSV file at approximately 30 Hz. The camera was operated at its maximum frame rate to preserve temporal resolution, thereby improving interpolation accuracy during subsequent data synchronisation and analysis.

Before starting the characterisation loops, preliminary inflations were performed and were excluded from the data processing, but served to run the membrane in and address the Mullins effect [19], which occurs during the first inflations of hyperelastic membranes. Indeed, Hyperelastic materials such as silicone and thermoplastic elastomers exhibit viscoelastic relaxation during their initial inflation cycles before setting a more repetitive behaviour after a few repeated cycles. Discarding the first few inflations ensured that the data captured the stable hysteresis characteristics of the HBMA.

Following the initial inflations, six characterisation loops were conducted. The first loop consisted of a full inflation up to 0.2 bar, while the subsequent five loops involved partial inflations with maximum pressure values of 0.15, 0.13, 0.12, 0.11, and 0.08 bar, respectively. These pressure values were chosen in view of characterising the ballooning actuator's positional response under controlled pressure variations. In each loop, the pressure was increased incrementally from 0 bar to the designated maximum value in steps of 0.005 bar, with waiting intervals of 5 s at each step to allow the system to stabilise. Upon reaching the target maximum pressure, an additional wait period of 5 s was applied before the pressure was decremented down to 0 bar in steps of 0.005 bar, again with 5-second intervals for stabilisation.

Pressure references of the regulator as well as the pressure measurements were respectively sent and acquired with the Portenta Machine Control, while the actuator position was computed in real time using MATLAB's Computer Vision Toolbox. Data collected from Arduino and MATLAB were synchronised using an LED programmed to blink at the start and end of the experiment.

C. Single Polynomial Fit Controller

The pressure measurements obtained from the characterisation experiment were plotted against the corresponding position values. The resulting equation was a 6th-degree polynomial. This best-fit curve, which disregards hysteresis effects, was used to derive pressure as a function of position and subsequently design the single polynomial fit controller. Polynomial fitting smooths the data and reduces the impact of outliers and thus makes trends easier to analyse since raw experimental data often contains noise due to sensor inaccuracies, environmental conditions, or hardware limitations.

$$P(H) = \sum_{n=0}^{6} a_n H^n \tag{1}$$

Equation (1) represents the Pressure-Position function for the Single Polynomial Fit controller, where P refers to the pressure and H is the position and a_n the coefficients of the polynomial. This equation is used in the next experimentation phase for position control.

D. Modified Prandtl-Ishlinskii (MPI) Controller

In order to obtain the mapping of pressure as a function of position for the MPI controller, it is first necessary to construct the MPI forward model. Unlike the polynomial fitting, the MPI forward model requires the independent variable (pressure) on the x-axis, since the play operators track the history of the input signal. The model output is computed as a weighted sum of these operators, capturing the causal, path-dependent nature of hysteresis. If the axes were swapped, the play operators could no longer follow the input history correctly, and the model would fail to capture the hysteresis behaviour. The method for building the MPI controller, based on this forward model, is described as follows.

To perform the MPI fitting, the data obtained from the characterisation was pre-processed by excluding the transient segment, subsequently smoothed to attenuate noise, and interpolated to yield a continuous representation with uniformly spaced samples along the axis. An MPI model was then fitted to the combined processed dataset in order to capture the hysteretic pressure-position behaviour of the balloon actuator. Before fitting, the dataset was normalised to the [0, 1] range using min-max scaling:

$$P_N = \frac{P - P_{min}}{P_{max} - P_{min}}, \qquad H_N = \frac{H - H_{min}}{H_{max} - H_{min}} \tag{2}$$

with P_N and H_N referring to the normalised pressure and normalised position respectively, and P, H the unscaled pressure and unscaled position.

The MPI operator extends the classical Prandtl-Ishlinskii (PI) model by augmenting the weighted superposition of play operators with cascaded dead-zone operators (DZ):

$$\widehat{H_N}(k) = \sum_{i=1}^{n_p} \omega_i \, \mathrm{Play}_{r_i}(P_N(k)) + \sum_{j=1}^{n_d} \nu_j \, S_{d_j}\left(\sum_{i=1}^{n_p} \omega_i \, \mathrm{Play}_{r_i}(P_N(k)) \right), \tag{3}$$

where $P_N(k)$ is the normalised input pressure at step k, $\mathrm{Play}_{r_i}(.)$ the play operator with threshold r_i, which models rate-independent hysteresis by preserving memory of past inputs, $S_{d_j}(.)$ is a dead-zone operator centred at d_j, which captures asymmetric features by suppressing small variations

around a threshold, ω_i and ν_j are the weights of the play and dead-zone operators, respectively, n_p and n_d are the numbers of play and dead-zone operators, and $\widehat{H_N}(k)$ is the predicted (estimated) normalised position.

The state update of each play operator is given by:

$$\begin{aligned}\mathrm{Play}_{r_i}(P_N)(k) = \max\{P_N(k) - r_i,\ \min[P_N(k) + r_i,\\ \mathrm{Play}_{r_i}(P_N)(k-1)]\}, \end{aligned} \tag{4}$$

which shows how the operator retains memory of inflation and deflation history.

Model parameters ω_i and ν_j were identified by solving a regularised non-linear least-squares problem:

$$\begin{aligned}\arg\min_{\{\omega_i,\nu_j\}} \left\| H_N - \widehat{H_N}(P_N;\omega,\nu)\right\|_2^2 \\ + \lambda_{\text{play}}\|\omega\|_2^2 + \lambda_{\text{dz}}\|\nu\|_2^2, \end{aligned} \tag{5}$$

where λ_{play} and λ_{dz} are Tikhonnov regularisation parameters that penalise excessively large play and dead-zone weights, improving robustness. Optimisation was performed using the trust-region reflective algorithm implemented in MATLAB's lsqonlin solver.

A grid search was performed across the number of play operators n_p, the number of dead-zone operators n_d, their thresholds, and regularisation strengths. Specifically, n_p and n_d were varied from 0 to 30, and each configuration was run with two random initialisations to reduce sensitivity to local minima. Candidate models were retained only if they satisfied boundedness and sparsity criteria (i.e., stable and no more than 20% near-zero coefficients). The final model was selected based on the lowest RMSE in de-normalised position. The selected configuration had $n_p = 28$ play operators and $n_d = 30$ dead-zone operators.

E. Feedforward position control and performances evaluation

For the position control experiment, the variation in displacement, achieved by the controllers, was carefully observed to evaluate performance and precision in maintaining the target position. The same setup shown in Fig. 3 was employed for both controllers except that this time, the camera was used solely for ground truth and was not integrated into the control algorithm. The Arduino board was reprogrammed to implement the feedforward control logic and to set desired position values of the soft ballooning membrane actuator. The controller executed a single up-down sweep of balloon position, starting from 3.5 mm to 20.5 mm and then back to 3.5 mm, in increments and decrements of 1 mm. Each step was held for 5 s to ensure the actuator reached steady state before proceeding.

For the single polynomial fit controller, the polynomial mapping disregarding the hysteresis, represented by equation (1) was embedded on the feedforward block on Fig. 1. The Arduino was programmed according to this mapping to generate the desired pressure P_r corresponding to the desired position H_r.

For the MPI controller, the Arduino Portenta was programmed to implement a real-time inverse of the fitted MPI forward model to compute the desired pressure P_r to achieve a target desired position H_r of the soft actuator without the need for lookup tables. The algorithm used the identified play and dead-zone parameters from fitted MPI model and employed a stateful bisection solver to invert the MPI operator. At each command step, the solver searched for the normalised pressure P_N such that

$$f(P_N) = \widehat{H_N}(P_N) - H_{N,r} = 0, \tag{6}$$

where $\widehat{H_N}(P_N)$ is the MPI forward operator and $H_{N,r}$ is the target normalised position. In practice, the solver stopped once the residual is sufficiently small, i.e.,

$$|f(P_N)| < \varepsilon, \tag{7}$$

where $\varepsilon = 0.05, \text{mm}$ (≈ 0.0022 in normalised units), ensuring the predicted position is within a small tolerance of the desired position. On the Arduino Portenta, convergence was consistently achieved in fewer than 10 iterations for all steps, well below the imposed cap of 64 iterations, and no divergence was observed.

To preserve hysteresis memory, the play-bank states were updated across iterations according to

$$\begin{aligned}\mathrm{Play}_{r_i}(P_N)(k) = \min\Big\{\max\big[P_N(k) - r_i,\\ \mathrm{Play}_{r_i}(P_N)(k-1)\big], P_N(k) + r_i\Big\}, \end{aligned} \tag{8}$$

thereby preventing inflation and deflation trajectories from collapsing into a single path and hence maintaining smooth and accurate motion. An analytical inverse was not implemented, since it is generally difficult to derive in closed form for complex hysteresis operators and can introduce stability issues. On the other hand, the numerical approach provided a robust and practical solution that accommodates non-linearities and remains feasible for real-time embedded control.

For both controllers, the Arduino board commanded the electro-pneumatic regulator to provide the computed pressure, while the displacement of the soft ballooning membrane was measured using the camera. The acquired images were recorded by MATLAB. In these position control experiments, pressure measurements were recorded by the external RS pressure sensor, with all data logged as CSV files by MATLAB.

To evaluate performance of the MPI controller under partial-range actuation, a position control experiment was conducted with a reduced maximum inflation of 10.5 mm, approximately half of the full-scale range. The actuator was commanded to follow a step trajectory from 3.5 mm to 10.5 mm in 1 mm increments, with a 5 s dwell time at each step before returning to 3.5 mm.

III. Results

A. Characterisation of the Soft Ballooning Actuator

This subsection presents the results obtained from the characterisation of the HBMA, with the objective of determining the pressure-position relationship for the two control

strategies. These functions are subsequently used in the position control experiments.

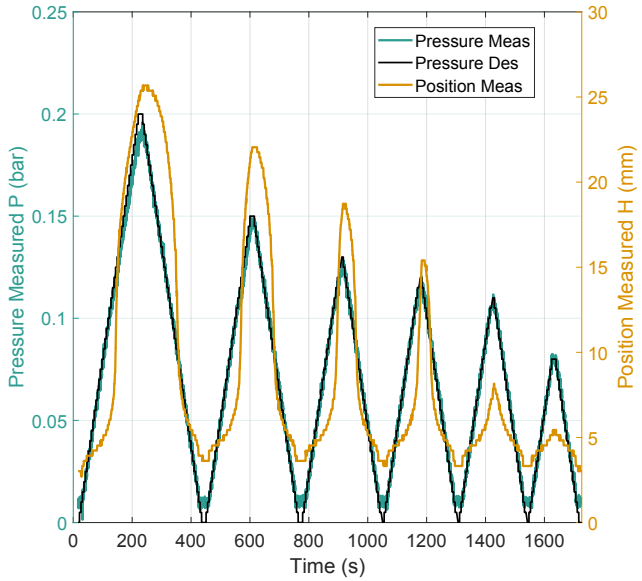

Fig. 4. Measured Pressure and Position during characterisation experiment.

Fig. 4 shows the measured pressure inside the HBMA during repeated actuation, along with the corresponding position values captured by the camera. Six actuations loops were recorded, with maximum pressures of 0.20, 0.15, 0.13, 0.12, 0.11 and 0.08 bar, respectively. For clarity, these loops are numbered from 1 (full inflation at 0.20 bar) to 6 (partial inflation at 0.08 bar). The measured position follows a similar trend: loops 1-4 exhibit the typical nonlinear ballooning behaviour, with a clear asymmetry between inflation and deflation due to hysteresis, while loops 5 and 6 appear nearly symmetrical, suggesting that the nonlinear 'ballooning effect' is not yet reached at these lower pressures. From the end of loop 1 onwards, the actuator settled to a residual position of around 3.3 mm for pressures below 0.01 bar, indicating the presence of a deadband region where no further position change was observed. The primary cause of this deadband region is the permanent deformation of the membrane. This effect is further compounded by the physical design of the HBMA, as the 2 mm cover prevents the camera from capturing any minimal deformation in that range. Consequently, desired positions below 3.5 mm were excluded in the position control experiments. Overall, both the pressure and position profiles follow approximately triangular trajectories over time, although the position response is smoother and exhibits a bell-shaped profile due to hysteresis.

Fig. 5 shows the variation of position with respect to pressure of the soft ballooning membrane and the fitted models using polynomial fit and MPI. The experimental data points are represented in grey markers.

As mentioned in II-C, for the single polynomial fit controller, the polynomial fitting was carried out on a graph whereby pressure was plotted against position hence obtain pressure as a function of Position, P(H). The orange curve

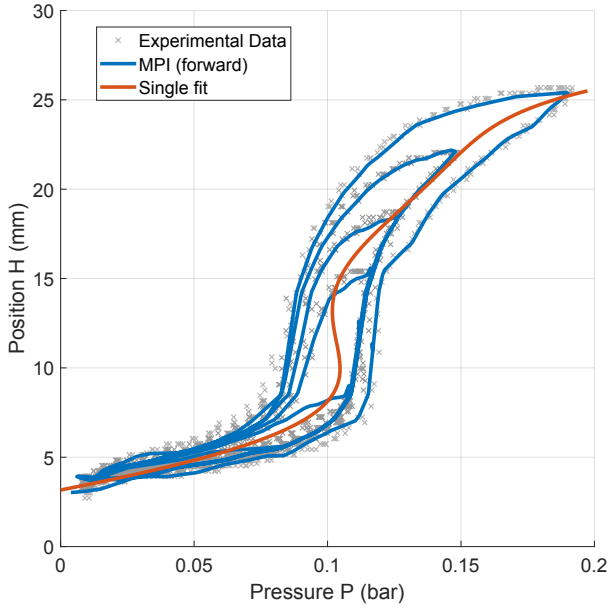

Fig. 5. Pressure against Position. MPI forward model and single fit polynomial.

represents the model used in the single polynomial fit controller, where a single polynomial is applied across the entire dataset. This fit provides a smooth, continuous representation of the pressure-position relationship, with coefficients listed in Table I and an RMSE of 0.0143 mm. However, it cannot capture the hysteresis and therefore averages the behaviour between inflation and deflation, leading to significant deviations in the mid-range (10-20 mm).

TABLE I
COEFFICIENTS OF THE POLYNOMIAL FIT FOR $P(H)$.

Term	Coefficient
H^6	5.537×10^{8}
H^5	-4.492×10^{6}
H^4	1.368×10^{4}
H^3	-1.854×10^{3}
H^2	9.227×10^{3}
H^1	1.578×10^{2}
H^0	-9.599×10^{2}

By contrast, the blue curves represent the MPI hysteresis model predictions for different inflation-deflation cycles. These curves closely matches the experimental grey data points, accurately capturing the nonlinear hysteretic behaviour of the actuator across multiple pressure-position loops. Unlike the single fit, they adapt to the path-dependent nature of the system, showing separate branches for inflation and deflation. The chosen MPI model had an RMSE value of 0.478 mm and the identified parameters, represented in 3 decimal places, are shown on Tables II and III.

For loop 1, the inflation cycle begins at approximately 3.5 mm with a corresponding pressure near 0 bar, and reaches a maximum position of 25.7 mm at 0.19 bar. This corresponds to an elongation of 109.4% relative to

TABLE II

PARAMETERS OF THE PI MODEL

n_p	1	2	3	4	5	6	7	8	9	10	11	12	13	14
r_i	0.000	0.010	0.026	0.046	0.069	0.094	0.122	0.151	0.182	0.215	0.249	0.284	0.321	0.359
w_i	0.467	-0.318	0.079	0.381	0.088	0.254	-0.142	0.048	0.211	-0.197	0.475	-0.314	-0.083	0.265
i	15	16	17	18	19	20	21	22	23	24	25	26	27	28
r_i	0.399	0.439	0.481	0.523	0.567	0.611	0.657	0.703	0.751	0.799	0.848	0.898	0.949	1.000
w_i	-1.362	2.449	-1.681	-1.086	3.335	-2.209	0.111	0.201	-0.266	0.288	-0.328	0.138	2.457	0.000

TABLE III

PARAMETERS OF THE DZ MODEL

n_d	1	2	3	4	5	6	7	8	9	10
d_j	0.000	0.015	0.035	0.059	0.084	0.111	0.140	0.169	0.200	0.232
w_s	-0.003	-0.393	-0.303	-0.146	-0.158	-0.230	0.625	0.027	-0.269	0.197
j	11	12	13	14	15	16	17	18	19	20
d_j	0.264	0.298	0.332	0.367	0.402	0.439	0.476	0.513	0.551	0.589
w_s	0.037	-0.062	-0.142	0.172	0.318	-0.020	0.090	1.343	4.599	-3.887
j	21	22	23	24	25	26	27	28	29	30
d_j	0.628	0.668	0.708	0.748	0.789	0.831	0.872	0.915	0.957	1.000
w_s	-0.984	-0.113	-0.547	0.115	-0.188	-0.502	-0.203	0.001	0.066	-0.161

the initial actuator height of 23.5 mm, highlighting the significant deformation achieved by the HBMA. During inflation, the curve initially rises steeply with increasing pressure, followed by a plateau region between roughly 8.5 and 14 mm, and then another steep increase until the peak position is attained. This plateau indicates a region where the ballooning membrane is stretching at roughly constant internal pressure (around 0.08 bar), even though its position is still increasing. This can be explained by a snap-through phenomenon (ballooning effect) [20], which can momentarily keep the internal pressure nearly constant while the structure transitions between stable shapes. On deflation, the loop traces a distinct lower path, illustrating a strong hysteresis, with the largest pressure-position offset observed in the mid-range (7-20 mm). Moreover, the smaller loops, particularly loops 2-5, further illustrate the actuator's behaviour within that offset region.

B. Controller Performance for Full Inflation

For the position control experiment, the Single Polynomial Fit controller was implemented using its equation, while the MPI controller employed the parameters of the fitted forward model. Their performance was evaluated in a full inflation trial, where the ballooning membrane was commanded to track a trajectory from 3.5 mm up to 20.5 mm and then back down. The desired and measured positions are compared in Fig. 6.

As shown in Fig. 6, the MPI controller followed the desired trajectory more closely than the Single Polynomial Fit controller. The MPI controller displayed a symmetric response characteristics during both inflation and deflation phases, whereas the Single Polynomial Fit controller lags during the early phase of inflation and then overshoots once the balloon enters its nonlinear deformation region. This highlights the limitations of the polynomial approximation, which averages out hysteresis effects.

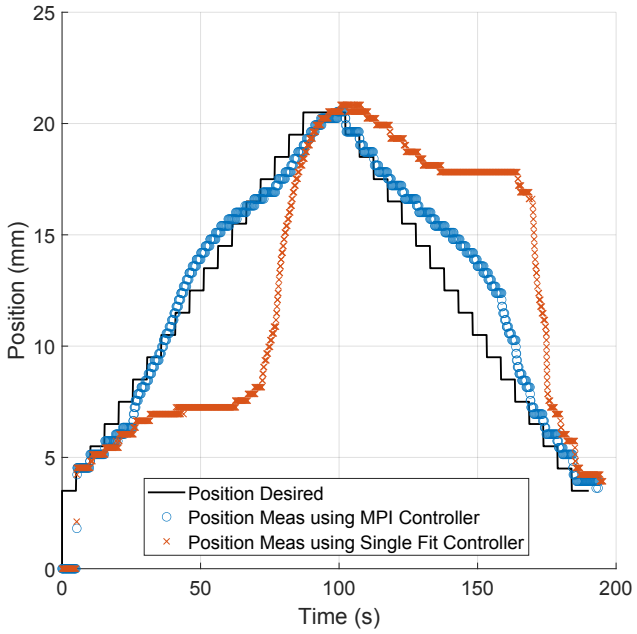

Fig. 6. Comparison of desired and measured positions for the Single Polynomial Fit and MPI controllers during full inflation and deflation.

To quantify the position tracking performance, the steady-state absolute errors, with transient regions excluded, are shown on Fig. 7. Sub-figure (A) corresponds to the inflation phase, and (B) shows the deflation phase.

During inflation (Fig. 7A), the MPI controller achieved a mean absolute error of 0.807 mm compared to 2.79 mm for the Single Polynomial Fit controller, representing a 71% reduction. The reported percentage improvement is computed from the ratio of mean absolute errors. Maximum errors for the MPI and Single Polynomial Fit controllers were 1.79 mm and 8.35 mm respectively. During deflation (Fig. 7B), the MPI controller again outperforms the Single Polynomial Fit

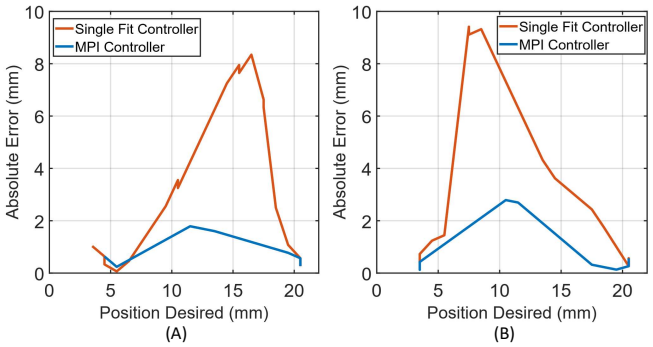

Fig. 7. Steady-state absolute position error between desired and measured positions for both controllers: (A) inflation phase, (B) deflation phase.

controller, with mean errors of 0.393 mm versus 1.34 mm (a 71% reduction), and maximum errors of 2.79 mm versus 9.41 mm. These results demonstrate that the MPI controller comprising of the inverse model provides significantly improved tracking, as it explicitly accounts for hysteresis and avoids the systematic bias inherent to the polynomial fit. Across repeated trials, the MPI controller maintained a low overall mean steady-state standard deviation of 0.134 mm (inflation: 0.157 mm; deflation: 0.119 mm), demonstrating high repeatability in its control performance.

C. Controller Performance for Half Inflation

To further assess the tracking capability of the MPI controller, this section evaluates its performance on a half inflation task, following a trajectory from 3.5 mm to 10.5 mm, and subsequently returning to 3.5 mm.

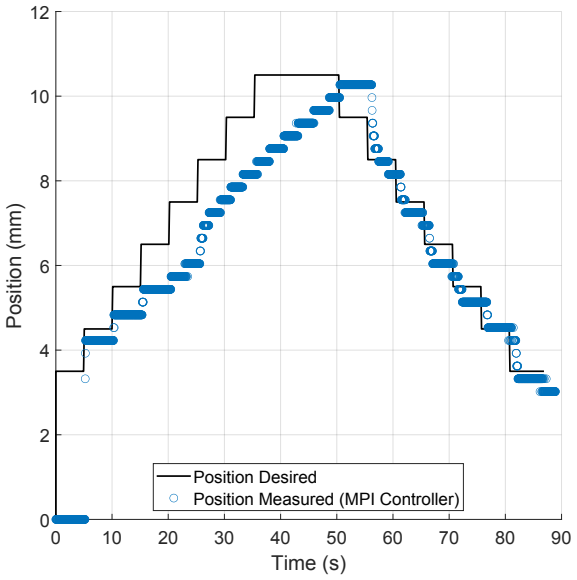

Fig. 8. Measured and desired positions for half-inflation using the MPI controller

Fig. 8 shows how the position measured using the MPI controller (represented by the blue curve) varied over time as the desired position (represented by the black line) changes. A small offset is observed between the blue curve and the black line during the inflation phase which was further reduced during the deflation phase.

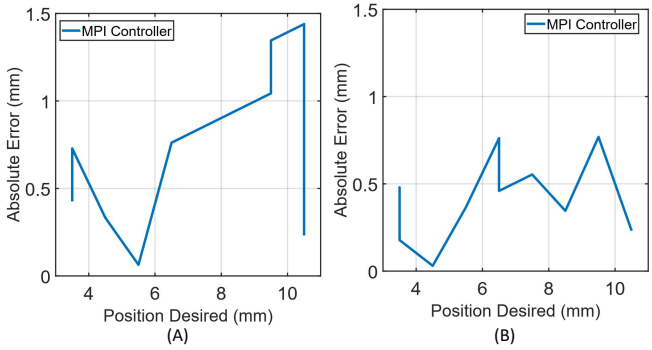

Fig. 9. Steady-state absolute position error during half-inflation between desired and measured positions for both controllers: (A) inflation phase, (B) deflation phase.

Fig. 9 illustrates the absolute position error during both inflation and deflation, highlighting the MPI controller's ability to achieve partial inflation up to 10.5 mm. The controller showed a mean absolute error of 0.972 mm during inflation and 0.399 mm during deflation. The maximum errors observed were 1.44 mm and 0.762 mm for the inflation and deflation phases, respectively. During inflation, the error fluctuated within 0-1.5 mm, whereas during deflation, it remained within 0-0.8 mm. These results indicate that the controller maintains consistent and accurate performance even at partial inflation levels. Furthermore, the overall mean steady-state standard deviation was 0.082 mm (inflation: 0.100 mm; deflation: 0.075 mm), confirming consistent behaviour across multiple cycles.

IV. Discussion and Conclusion

This paper studied the performance and limitations of feedforward position control for an HBMA, focusing on how accuracy can be improved by explicitly modelling hysteresis. Following characterisation of the actuator's nonlinear pressure-position behaviour, two feedforward position control strategies were compared: a Single Polynomial Fit controller, which approximates the pressure-position relation with high-order polynomial and disregards hysteresis, and an MPI controller, which incorporates a Modified Prandtl-Ishlinskii model to represent and invert hysteresis. The MPI inversion was implemented numerically on the embedded controller using a stateful bisection solver, preserving hysteresis history between commands to ensure smooth motion. The results demonstrate that MPI-based hysteresis inversion can be implemented in real time on embedded hardware for ballooning membrane actuators without auxiliary position sensing. Experimental results showed that, for full inflation, the MPI controller substantially improved position accuracy, under pressure regulation, compared to the Single Polynomial Fit controller. Moreover, the MPI controller produced a more symmetrical position responses behaviour across inflation and deflation phases. A symmetrical response simplifies prediction and enhances repeatability compared

to an asymmetric one. Steady state absolute mean error plots further confirmed that the MPI controller significantly reduced position tracking error by 71% relative to the Single Polynomial Fit controller. Based on these results, it can be concluded that the MPI hysteresis model is well-suited to capture the non-linear and path-dependent behaviour of the HBMA, addressing its hysteresis and mitigating, albeit not fully, the ballooning effect inherent to hyperelastic membranes.

Overall, feedforward position control of ballooning membranes remains a promising research direction for soft robotics particularly when combined with hysteresis compensation. Feedforward hysteresis-compensated control enables a range of practical applications. For instance, multiple HBMAs, as described in this paper, could be grouped and stacked to form snake-like continuum robots that rely on feedforward control to achieve complex motions without the need for external feedback devices. In minimally invasive medical tools, such as catheters or endoscopes, bulky sensors cannot be embedded, but feedforward control allows actuators to reach target shapes or elongations based solely on pressure commands. Similarly, wearable devices and rehabilitation exosuits benefit from lightweight, low-power designs, where feedforward control reduces the need for distributed high-bandwidth sensors while still compensating for actuator hysteresis. Adaptive soft grippers also benefit, as actuators can predictably wrap around fragile objects without over-squeezing, minimising reliance on force feedback. Finally, for multi-segment continuum robots, fully sensorised architectures are challenging; feedforward control allows coordinated actuation across many segments using only pressure commands, facilitating scalable designs.

Moreover, the feedforward approach reduces reliance on external measurement systems, such as cameras or optical trackers, which are often used to capture actuator motion. Avoiding such devices minimises system wiring and decreases dependence on environmental factors such as lighting, image segmentation, an unobstructed view of the actuator, or workspace accessibility. This makes the system more suitable for environments that could interfere with measurements, such as cluttered, flooded, or hazardous settings. Future work will investigate alternative actuation strategies, such as flow regulation, incorporate time-dependent viscoelastic effects of the membrane, and evaluate generalisation across different membranes and pressure ranges to further improve accuracy and robustness during prolonged operation and under varying operating conditions such as non-monotonic actuation.

REFERENCES

[1] M. Zhu, S. Biswas, S. I. Dinulescu, N. Kastor, E. W. Hawkes, and Y. Visell, "Soft, wearable robotics and haptics: Technologies, trends, and emerging applications," *Proc. IEEE*, vol. 110, no. 2, pp. 246–272, Feb. 2022.

[2] M. Cianchetti, C. Laschi, A. Menciassi, and P. Dario, "Biomedical applications of soft robotics," *Nature Reviews Materials*, vol. 3, no. 6, pp. 143–153, May 2018.

[3] M. Pan, C. Yuan, X. Liang, T. Dong, T. Liu, J. Zhang, J. Zou, H. Yang, and C. Bowen, "Soft actuators and robotic devices for rehabilitation and assistance," *Adv. Intell. Syst.*, vol. 4, no. 4, p. 2100140, 2022.

[4] M. S. Xavier, C. D. Tawk, A. Zolfagharian, J. Pinskier, D. Howard, T. Young, J. Lai, S. M. Harrison, Y. K. Yong, M. Bodaghi, and A. J. Fleming, "Soft pneumatic actuators: A review of design, fabrication, modeling, sensing, control and applications," *IEEE Access*, vol. 10, pp. 59 442–59 485, 2022.

[5] S. Liu, L. Wang, Z. Qian, D. Liu, W. Zhu, S. Tang, X. Zhao, W. Yang, Y. Lu, J. Yi, J. S. Dai, and Z. Wang, "Single pump-valve pneumatic actuation with continuous flow rate control for soft robots," *IEEE Robot. Autom. Lett.*, vol. 10, no. 3, pp. 2399–2406, Mar. 2025.

[6] M. A. Horvath, I. Wamala, E. Rytkin, E. Doyle, C. J. Payne, T. Thalhofer, I. Berra, A. Solovyeva, M. Saeed, S. Hendren, E. T. Roche, P. J. del Nido, C. J. Walsh, and N. V. Vasilyev, "An intracardiac soft robotic device for augmentation of blood ejection from the failing right ventricle," *Ann. Biomed. Eng.*, vol. 45, no. 9, pp. 2222–2233, 2017. [Online]. Available: https://doi.org/10.1007/s10439-017-1855-z

[7] J. Shi, K. Borvorntanajanya, K. Chen, E. Franco, and F. R. y. Baena, "Design, control, and evaluation of a novel soft everting robot for colonoscopy," *IEEE Trans. Robot.*, vol. 41, pp. 4843–4859, 2025.

[8] M. Ismayilov, J. Merlin, C. Bergeles, and L. Lindenroth, "A generalized modeling approach to liquid-driven ballooning membranes," in *Proc. IEEE Int. Conf. Soft Robot. (RoboSoft)*, Apr. 2025, pp. 1–7.

[9] N. Herzig, J. Jones, E. Perez-Guagnelli, and D. D. Damian, "Model and validation of a highly extensible and tough actuator based on a ballooning membrane," in *Proc. IEEE Int. Conf. Robot. Autom. (ICRA)*, May 2021, pp. 11 961–11 967.

[10] S. Konishi, F. Kawai, and P. Cusin, "Thin flexible end-effector using pneumatic balloon actuator," *Sens. Actuators A Phys.*, vol. 89, no. 1, pp. 28–35, 2001.

[11] U. H. Ko, V. Kumar, B. Rosen, and S. Varghese, "Characterization of bending balloon actuators," *Front. Robot. AI*, vol. 9, 2022. [Online]. Available: https://www.frontiersin.org/journals/robotics-and-ai/articles/10.3389/frobt.2022.991748

[12] R. F. Reinhart, Z. Shareef, and J. J. Steil, "Hybrid analytical and data-driven modeling for feed-forward robot control," *Sensors*, vol. 17, no. 2, 2017.

[13] J. Qu, K. Khan, S. Meng, and A. Muliana, "Modeling nonlinear viscoelastic responses of flexible composites for soft robotics applications," *Mech. Adv. Mater. Struct.*, vol. 30, no. 14, pp. 2793–2805, 2023. [Online]. Available: https://doi.org/10.1080/15376494.2022.2063460

[14] H. Hu and R. Ben Mrad, "On the classical preisach model for hysteresis in piezoceramic actuators," *Mechatronics*, vol. 13, no. 2, pp. 85–94, Feb. 2003. [Online]. Available: https://www.sciencedirect.com/science/article/pii/S0957415801000435

[15] M. Al Janaideh, J. Mao, S. Rakheja, W. Xie, and C.-Y. Su, "Generalized prandtl-ishlinskii hysteresis model: Hysteresis modeling and its inverse for compensation in smart actuators," in *Proc. 47th IEEE Conf. Decis. Control (CDC)*, Dec. 2008, pp. 5182–5187.

[16] G. Flores, N. Aldana, and M. Rakotondrabe, "Model predictive control based on the generalized bouc-wen model for piezoelectric actuators in robotic hand with only position measurements," *IEEE Control Syst. Lett.*, vol. 6, pp. 2186–2191, 2022.

[17] V. Hassani, T. Tjahjowidodo, and T. N. Do, "A survey on hysteresis modeling, identification and control," *Mech. Syst. Signal Process.*, vol. 49, no. 1, pp. 209–233, 2014.

[18] S. Xie, J. Mei, H. Liu, and Y. Wang, "Hysteresis modeling and trajectory tracking control of the pneumatic muscle actuator using modified prandtl–ishlinskii model," *Mech. Mach. Theory*, vol. 120, pp. 213–224, 2018. [Online]. Available: https://www.sciencedirect.com/science/article/pii/S0094114X17308169

[19] L. Mullins, "Softening of rubber by deformation," *Rubber Chem. Technol.*, vol. 42, no. 1, pp. 339–362, Mar. 1969. [Online]. Available: https://doi.org/10.5254/1.3539210

[20] J. T. B. Overvelde, T. Kloek, J. J. A. D'haen, and K. Bertoldi, "Amplifying the response of soft actuators by harnessing snap-through instabilities," *Proc. Natl. Acad. Sci. USA*, vol. 112, no. 35, pp. 10 863–10 868, 2015. [Online]. Available: https://www.pnas.org/doi/abs/10.1073/pnas.1504947112